Canonical dynamics of the Nosé oscillator: Stability, order, and chaos

Harald A. Posch, William G. Hoover,* and Franz J. Vesely

Institut für Experimentalphysik, Universität Wien, Boltzmanngasse 5, A-1090 Vienna, Austria

Nosé has developed many-body equations of motion designed to reproduce Gibbs's canonical phase-space distribution. These equations of motion have a Hamiltonian basis and are accordingly time reversible and deterministic. They include thermodynamic temperature control through a single deterministic friction coefficient, which can be thought of as a control variable or as a memory function. We apply Nosé's ideas to a single classical one-dimensional harmonic oscillator. This relatively simple system exhibits both regular and chaotic dynamical trajectories, depending on the initial conditions. We explore here the nature of these solutions by estimating their fractal dimensionality and Lyapunov instability. The Nosé oscillator is a borderline case, not sufficiently chaotic for a fully statistical description. We suggest that the behavior of only slightly more complicated systems is considerably simpler and in accord with statistical mechanics.

I. INTRODUCTION AND MOTIVATION

During the past ten years an intensive effort has been made to use computers in the simulation of many-body systems in nonequilibrium states.[1] A major difficulty in achieving this goal had been the lack of useful controls over the thermodynamic independent variables. It is necessary to control temperature or pressure or energy in order to simulate nonequilibrium steady states far from equilibrium. The techniques of control theory can be applied to this problem, adding arbitrary "control forces" or "constraint forces" designed to maintain thermodynamic variables fixed. Some of these same constraint forces are suggested by classical mechanics. Gauss, for instance, made the reasonable suggestion that constraint forces should be made as small as is possible, in a least-squares sense. The resulting principle of least constraint[2] is the most general formulation of classical mechanics. This principle leads to frictional forces, linear in the momentum, of the same form familiar from control theory.[3] Much more recently, Nosé has suggested a frictional force designed to reproduce the canonical (constant thermodynamic temperature) and isobaric (constant thermodynamic pressure) phase-space distributions in equilibrium systems.[4,5] Nosé's equations of motion incorporate "integral control" in which the friction coefficient, or "control variable," depends linearly on the integrated history of the system's kinetic energy.

Unlike hydrodynamic frictional forces, Gauss's and Nosé's forces are time reversible. In fact, even far from equilibrium, the new equations, like Newton's, are purely deterministic and reversible.

Canonical ensemble equilibrium properties are not at all mysterious or hard to compute. There already exist many practical schemes for determining the thermodynamic and structural properties of many-body systems with good accuracy.[6] Thus the new schemes have little to offer in the way of improving equilibrium simulations. Instead, Gauss's and Nosé's ideas are particularly promising because they suggest approaches to classes of problems in nonequilibrium and quantum-mechanical simulation for which no useful theories exist. They also suggest ways of simplifying and unifying deterministic and stochastic dynamics through the use of deterministic driving forces.

These ideas have already proved their usefulness in the study of nonequilibrium systems. The new equations make it possible to simulate, and to analyze theoretically, systems connected to thermal or mechanical reservoirs without the need for stochastic or irreversible forces. It is remarkable that this has been achieved with time-reversible equations. Thus a movie of a physically irreversible process described with a Gaussian or Nosé thermostat represents accurately the mathematical formal solution of the equations of motion only in the forward direction. Because the backward direction corresponds to an entropy decrease, it cannot be observed in any finite-precision computation and the reversed movie represents a fictional trajectory.

Gauss's and Nosé's equations of motion have been applied to the study of fluid and solid diffusion,[2,7] viscosity,[8,9] and heat conduction[10,11] with computer simulation and to the nonlinear generalization of linear response theory[12,13] required to describe systems far from equilibrium.

In order to characterize these new dynamical approaches and to assist the development of the theory, it is essential to study their application to the simplest possible prototypical systems. In this way the advantages of the new methods can be exploited and the disadvantages surmounted. Thus two-body[7–9] and three-body[10] nonequilibrium systems have been simulated using Gaussian and Nosé dynamics.

To help assess these new developments in nonequilibrium molecular dynamics we study here the one-dimensional harmonic oscillator using Nosé's canonical equations of motion.[14] This is a problem with three time-dependent variables, the coordinate q, the momentum p, and the friction coefficient ζ. Each of these obeys a first-order differential equation of motion. The oscillator exhibits many of the familiar features found earlier in

the studies of the Lorenz,[15] Henon-Heiles,[16] and double-pendulum[17] systems. The last two of these problems are mathematically reversible, like the Nosé oscillator, and restricted to a three-dimensional subspace of a four-dimensional phase space by an energy integral of the equations of motion.

In the limiting cases of very weak and very strong thermostats, the motion of the Nosé oscillator can be understood analytically. In the intermediate, chaotic region, Poincaré maps cutting the three-dimensional phase space (q, p, ζ) are useful tools. The accessible part of this phase space is unbounded in extent as a consequence of the logarithmic form of the thermostat potential. For experimentally accessible times, however, the trajectory is always confined to a rather small phase-space volume around the origin regardless of the initial conditions. The solution of the Nosé oscillator problem thus behaves like a strange attractor familiar from the study of dissipative systems. We have characterized the chaotic regime in terms of the Lyapunov exponent and fractal dimensionality of this "strange attractor." The motion of the phase point in $\{q, p, \zeta\}$ space provides many attractive pictures.

The oscillator calculations suggest the need for some caution in applying Nosé's dynamics to the simulation of statistical-mechanical systems. Just as in the case of Newtonian mechanics, it appears that Nosé and Gaussian mechanical systems, if they are simple enough, are inconsistent with the usual statistical description. On the other hand, it is possible, and may be even likely, that the complexity associated with fractals and strange attractors is not generally important. Very simple systems with additional topological complexity produce behavior we have been unable to distinguish from truly (quasi-)ergodic trajectories. This includes a problem which requires only a three-variable phase space for its description, namely a particle moving in a two-dimensional potential at constant kinetic energy. Of course, a foolproof test for ergodicity is still lacking. Perhaps such a test will emerge from the computational analysis of simple systems like the Nosé oscillator.

In Sec. II we describe three equivalent forms of Nosé's equations of motion. We apply them there to the only case for which an exact solution is known, a classical ideal gas.

In Sec. III we consider a classical one-dimensional harmonic oscillator, as described by Nosé's equations of motion. We concentrate there on analyzing simple limiting cases, the recurrent and nearly recurrent orbits which occur in the weak- and strong-coupling limits.

In Sec. IV we present a numerical study of the chaotic regime which lies between the limiting cases discussed in Sec. III. The behavior found is discussed using standard techniques—Lyapunov exponents and Poincaré phase-space sections. Many of the phase portraits of the simple oscillator are surprisingly pretty.

In Sec. V we consider two slightly more complicated systems, using the same equations of motion, a two-body problem with Nosé dynamics and a two-body problem using Gaussian dynamics. These problems involve, respectively, five and three phase-space variables. In both cases it appears that the behavior is different from that of the Nosé oscillator, so that statistical mechanics can probably be applied to most systems of interest.

Section VI is a short summary of the work presented here together with speculations on extensions of Nosé's work to treat more complicated kinds of physical problems.

II. ISOTHERMAL EQUATIONS OF MOTION: NOSÉ'S DYNAMICS

Nosé succeeded in reproducing Gibbs's canonical distribution from isoenergetic dynamics. To do this, he considered an augmented system with an explicit one-parameter heat bath. The equivalence of the dynamical phase-space distribution with Gibbs's canonical distribution has been established in two somewhat different ways: by integrating the microcanonical distribution over the heat-bath variable and its conjugate momentum[4,5] or by direct calculation of the extended phase-space flow generated by the dynamics.[14] For either proof it is necessary to assume that the augmented system behaves in a quasiergodic way, approaching closely all accessible points in phase space during the course of a long-time trajectory.

Nosé's approach can be generalized in many ways. For instance, equations of motion which control moments of the velocity distribution beyond the second can be considered. These can be applied to the study of energy-sensitive processes, such as shock-wave-induced chemical reactions, but we will not consider them here. Likewise, by developing equations of motion designed to reproduce known quantum expectation values, classical mechanics could be generalized to estimate unknown quantum properties. We developed neither of these straightforward generalizations of Nosé's ideas here.

Nosé's many-body Hamiltonian,

$$H_N = \sum_i \frac{\mathbf{P}_i^2}{2m_i s^2} + \Phi + \alpha \frac{P_s^2}{2} + NDk_B T \ln s , \qquad (1)$$

can be made the basis for many different forms of isothermal canonical equations of motion. In (1), D is the dimensionality of the N-particle system. The momentum P_s, with an effective mass $1/\alpha$, is conjugate to the dimensionless "time-scale" variable s. We discuss the meaning of scaled time below. The thermodynamic temperature T is coupled to the time development of the trajectories through the kinetic energy. The potential energy Φ, which depends upon coordinates $\mathbf{Q}_i$, represents the interactions of all particles making up the system. The time-scale or "effective-mass" variable s, and its conjugate momentum P_s, interact collectively with all of the degrees of freedom $\{\mathbf{Q}_i, \mathbf{P}_i\}$ of the particles. To make the present work self-contained, we will first describe the series of transformations linking the three forms of Nosé's equations of motion together. We include the solution for the ideal-gas case. The reader wanting more details should consult Nosé's original work as well as Ref. 14.

The equations of motion from the Hamiltonian (1) are

$$\dot{\mathbf{Q}}_i = \mathbf{P}_i/m_is^2, \quad \dot{\mathbf{P}}_i = \mathbf{F}_i \tag{2}$$

$$\dot{s} = \alpha P_s, \quad \dot{P}_s = \frac{1}{s}\sum_i\left[\frac{\mathbf{P}_i^2}{m_is^2} - Dk_BT\right].$$

For any solution of these equations the Hamiltonian (1) is the corresponding constant of the motion. Other forms of the equations of motion can be obtained from (2) by time scaling. Nosé suggested scaling the time in such a way that all the time derivatives in (2), expressed in terms of "scaled-time" derivatives, are made larger by a factor of s. The time scale varies such that $(d/dt)_{\text{new}} = s(d/dt)_{\text{old}}$ or, equivalently, so that $dt_{\text{new}} = dt_{\text{old}}/s$. Expressed in terms of derivatives with respect to the scaled time t_{new} and still using the dot notation for these new time derivatives, the equations (2) become

$$\dot{\mathbf{Q}}_i = \mathbf{P}_i/m_is, \quad \dot{\mathbf{P}}_i = s\mathbf{F}_i, \tag{3}$$

$$\dot{s} = s\alpha P_s, \quad \dot{P}_s = \sum_i\left[\frac{\mathbf{P}_i^2}{m_is^2} - Dk_BT\right],$$

where $\mathbf{F}_i = -\nabla_i\Phi$ is the force acting on particle i. It needs to be emphasized that the trajectories in $\mathbf{Q}\mathbf{P}sP_s$ space from (2) and (3) are identical, but they are traced out at different rates. The time-scale variable s (which could also be thought of as an effective mass ms^2) just plays the role of a clock. Any other clock could be used with any dependence whatsoever on $\mathbf{Q}_i$, $\mathbf{P}_i$, s, and P_s or even on variables outside that set. Still the trajectories would trace out the same curve in $\mathbf{Q}\mathbf{P}sP_s$ space. Both sets of equations (2) and (3) clearly have the same constant of the motion, H_N.

An even simpler description of the motion is obtained by transforming to new variables $\mathbf{q}_i$, $\mathbf{p}_i$, and ζ according to

$$\mathbf{q}_i = \mathbf{Q}_i, \quad \mathbf{p}_i = m_i\dot{\mathbf{q}}_i = \frac{\mathbf{P}_i}{s}, \quad \zeta = \frac{d\ln s}{dt} = \alpha P_s. \tag{4}$$

In this representation the equations of motion assume the form

$$\dot{\mathbf{q}}_i = \mathbf{p}_i/m_i,$$

$$\dot{\mathbf{p}}_i = \mathbf{F}_i - \zeta\mathbf{p}_i, \tag{5}$$

$$\dot{\zeta} = \alpha\sum_i(\mathbf{p}_i^2/m_i - Dk_BT),$$

which simplifies the dynamical description by reducing the phase-space dimensionality by one. The friction coefficient ζ couples the N-particle system to a heat bath maintaining a constant temperature T. Equation (1) is still a constant of the motion and may be expressed in terms of our new variables according to

$$H = \sum_i\mathbf{p}_i^2/2m_i + \Phi + Nk_BT\int_0^t\zeta(t')dt' + \zeta^2/2\alpha. \tag{6}$$

Using the equations of motion (5), only $\mathbf{q}_i$, $\mathbf{p}_i$, and ζ (or $P_s = \zeta/\alpha$) are given by the solution, where $\mathbf{p}_i$ in (5) is the original Nosé $\mathbf{P}_i$ divided by s. This solution is independent of H. But, from the initial value of the Hamiltonian (1), in which the integral over time does not occur, s may be obtained,

$$s = \exp\left[\left[H_N - \Phi - \zeta^2/2\alpha - \sum_i\mathbf{p}_i^2/2m_i\right]\Big/ Nk_BT\right], \tag{7}$$

from which the momenta in the Nosé description can be calculated.

The dynamical equations are relatively complicated for most systems, yielding a chaotic motion even for the prototypical stable system, a harmonic oscillator. The D-dimensional N-particle ideal gas can be worked out in detail, as Nosé emphasized. In that case all of the forces $\mathbf{F}_i$ are zero and it is convenient to introduce the variable $X = \ln[\sum(\mathbf{p}_i^2/m_i)/DNk_BT]$. Equations (5) reduce to a simple second-order differential equation for X:

$$\ddot{X} = -2\alpha DNk_BT[\exp(X) - 1]. \tag{8}$$

Thus the kinetic energy behaves like a particle oscillating in a nonlinear Toda potential

$$\Phi_{\text{eff}} = 2\alpha DNk_BT[\exp(X) - 1 - X] \tag{9}$$

with a definite frequency and amplitude. For small α the variable X oscillates with a frequency of order $\sqrt{\alpha}$. The momentum of each particle oscillates in magnitude but remains fixed in direction. Thus the Nosé thermostat is not sufficiently powerful to force a gas into the canonical distribution in velocity space. The lack of a closed-form integral for motion in the ideal-gas case (8) suggests that only perturbation or numerical approaches will be useful for more complicated (i.e., nonzero) potentials.

III. HARMONIC-OSCILLATOR NOSÉ MECHANICS: REGULAR TRAJECTORIES

The one-dimensional classical harmonic oscillator is qualitatively a much more complex problem than is the ideal gas. The interaction between the fundamental oscillator frequency and the frequency associated with the heat-bath variable s leads to a wide variety of regular and not-so-regular trajectories. For simplicity we introduce reduced variables by choosing m, $\sqrt{m/k}$, and $\sqrt{k_BT/k}$ as units for the mass, time, and length scales, respectively, where m is the mass and k the spring constant of the oscillator. If the same symbols are used for the original and reduced quantities, the Hamiltonian (1) for the one-dimensional Nosé oscillator can be written as

$$H_N = \frac{Q^2}{2} + \frac{P^2}{2s^2} + \ln s + \frac{\alpha P_s^2}{2}. \tag{10}$$

After time scaling by the scale variable s, the equations of motion follow from (3):

$$\dot{Q} = P/s, \quad \dot{P} = -Qs,$$

$$\dot{s} = s\alpha P_s, \quad \dot{P}_s = P^2/s^2 - 1. \tag{11}$$

Transformation to new variables as in (4),

$$q = Q, \quad p = P/s, \quad \zeta = \frac{d\ln s}{dt} = \alpha P_s, \tag{12}$$

leads to the alternative q, p, ζ representation of the Nosé

oscillator, for which the Hamiltonian (6) may be transcribed:

$$H = \frac{q^2}{2} + \frac{p^2}{2} + \frac{\zeta^2}{2\alpha} + \int_0^t \zeta(t')dt' .$$ (13)

The equations of motion (5) assume the particularly simple form

$$\dot{q} = p, \quad \dot{p} = -q - \zeta p, \quad \dot{\zeta} = \alpha(p^2 - 1) .$$ (14)

The oscillator coordinate and momentum are q and p. The friction coefficient maintaining the reduced temperature equal to 1 is ζ. It is obvious from (13) and (14) that the physics of the Nosé oscillator depends on a single parameter, the coupling parameter α.

There is an extensive literature recommending methods for finding the solution of such equations as asymptotic series in $\epsilon = \sqrt{\alpha}$, valid for times small with respect to $1/\epsilon$.[18,19] But it is actually considerably simpler, given the simple structure of the equations, to guess the form of the solution from numerical solutions. In the analysis it is convenient to use an energy $E' = (q^2 + p^2 + \zeta^2/\alpha)/2$ so that $\dot{E}' = -\zeta$. As an example we consider the case $H = 1$ with the initial conditions $q_0 = 0$, $p_0 = \sqrt{2}$, $\zeta_0 = 0$. The Fourier-series solution has the form

$$E' = 1 - \frac{1}{2}(\epsilon \sin t)^2 + \frac{3}{8}[\epsilon \sin(\epsilon t/2)]^2$$
$$- \frac{1}{16}\epsilon^4 t \sin(2t) + O(\epsilon^4)$$ (15)

for times less than $2\pi/\epsilon$. The error includes terms of order $\epsilon^6 t^2$. For solving the equations of motion (14) we used Hamming's predictor-corrector method of order 4.[20] With a time step of 0.001 and double-precision arithmetic on an HP-A600+ computer, we had no difficulty in generating solutions with the constant of the motion (13) fixed to eight figures up to 2×10^6 time steps ($\alpha = 1$).

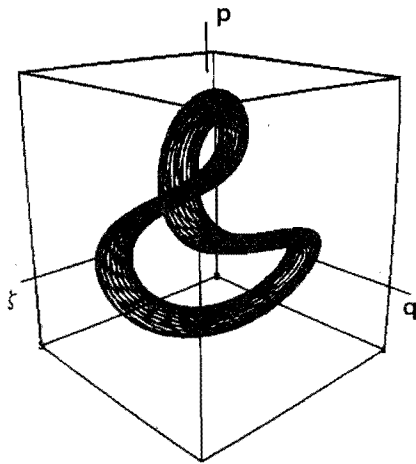A Newtonian oscillator traces out an ellipse with two turning points for q and for p at which p and q vanish.

FIG. 1. Regular trajectory of the Nosé oscillator for $\alpha = 1$. The q,p,ζ axes are only drawn outside the cube with the origin at the center. Initial condition: $q_0 = 0$, $p_0 = 2$, $\zeta_0 = 0$. The range of scales is indicated by the edges of the cube: $-1 \le q \le 1$, $-3 \le p \le 3$, $-8 \le \zeta \le 8$.
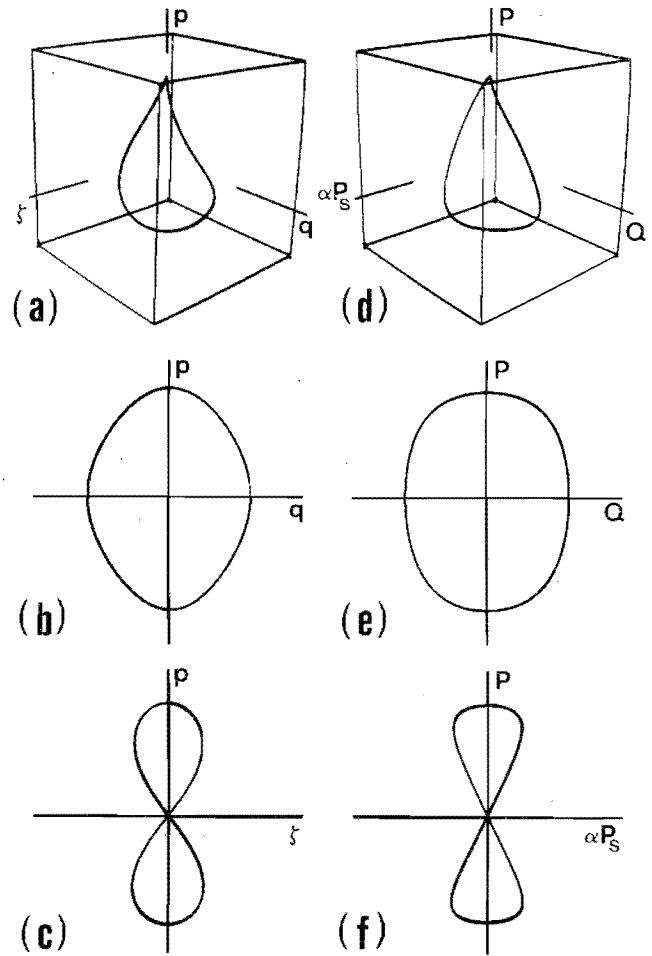

FIG. 2. Periodic orbit of the Nosé oscillator for $\alpha = 1$ and $n = 1$, where n is the number of maxima of p. (a) shows a perspective view of the trajectory in the phase space of the modified q,p,ζ representation, whereas (d) depicts the same trajectory in the original Nosé variables Q,P,s,P_s. The coordinate axes are only drawn outside the cube with the origin at its center. Initial condition: (a)–(c), $q_0 = 0$, $p_0 = 1.55$, $\zeta_0 = 0$; (d)–(f), $Q_0 = 0$, $P_0 = 1.55$, $s_0 = 1$, $P_{s0} = 0$. The indicated range of scales corresponds to the edges of the cube for (a) and (d) and to the lengths of the axes for the projections: (a)–(c), $-2 \le q \le 2$, $-2 \le p \le 2$, $-2 \le \zeta \le 2$; (d)–(f), $-2 \le Q \le 2$, $-2 \le P \le 2$, $-2 \le \alpha P_s \le 2$.

This Newtonian ellipse is transformed into a KAM (Kolmogorov-Arnold-Moser) torus for small values of the perturbation α. As the trajectory spirals around this torus, ζ oscillates at twice the fundamental oscillator frequency. This follows from the quadratic driving terms in the equation of motion for ζ, which changes sign four times per cycle as p passes through the values 1 and -1.

For larger values of the perturbation parameter α both regular and chaotic solutions can be generated. The latter will be discussed in the following section. The regular solutions are generally quasiperiodic and trace out KAM tori in phase space. An example is shown in Fig. 1 for $\alpha = 1$. For particular sets of initial conditions the tori degenerate into periodic orbits. In the following a classification of the possible reentrant orbits is given. Without loss
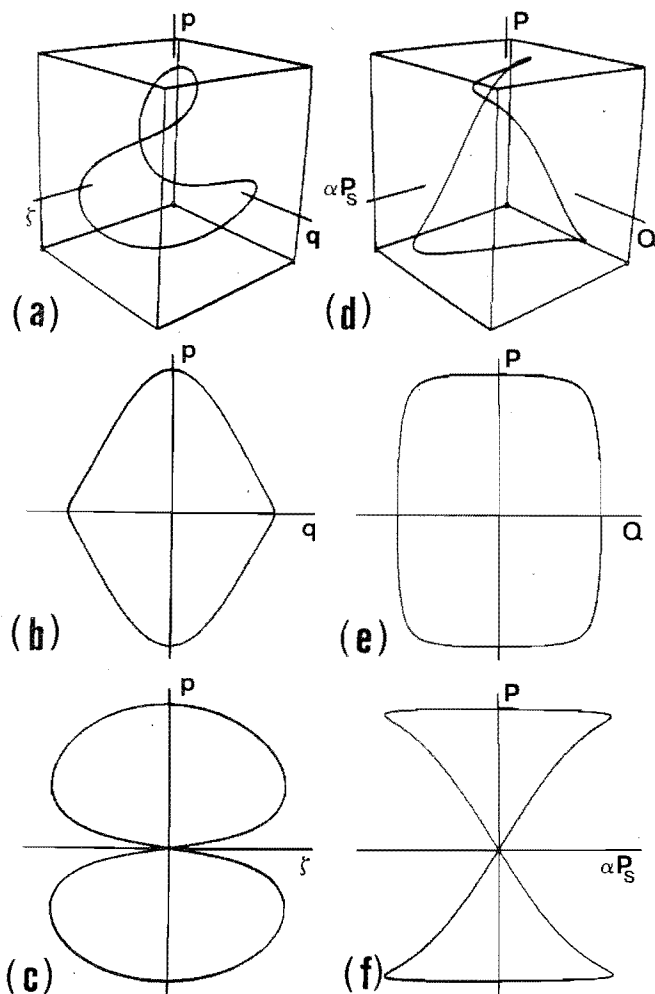
(a) (d) (b) (e) (c) (f)

FIG. 3. As in Fig. 2 for $\alpha = 10$ and $n = 1$. Initial condition: (a)–(c), $q_0 = 0$, $p_0 = 2.25$, $\zeta_0 = 0$; (d)–(f), $Q_0 = 0$, $P_0 = 2.25$, $s_0 = 1$, $P_{s0} = 0$. Scales: (a)–(c), $-0.8 \leq q \leq 0.8$, $-2.5 \leq p \leq 2.5$, $-6 \leq \zeta \leq 6$; (d)–(f), $-0.8 \leq Q \leq 0.8$, $-2.5 \leq P \leq 2.5$, $-6 \leq \alpha P_s \leq 6$.

FIG. 4. As in Fig. 2 for $\alpha = 10$ and $n = 5$. Initial condition: (a)–(c), $q_0 = 0$, $p_0 = 1.036$, $\zeta_0 = 0$; (d)–(f), $Q_0 = 0$, $P_0 = 1.036$, $s_0 = 1$, $P_{s0} = 0$. Scales: (a)–(c), $-5 \leq q \leq 5$, $-3 \leq p \leq 3$, $-6 \leq \zeta \leq 6$; (d)–(f), $-5 \leq Q \leq 5$, $-2.5 \leq P \leq 2.5$, $-6 \leq \alpha P_s \leq 6$.

of generality we restrict ourselves to the symmetrical initial conditions $q_0 = 0$, $p_0 \neq 0$, $\zeta_0 = 0$.

In Fig. 2 a perspective view of the simplest possible reentrant orbit for $\alpha = 1$ is shown both in the modified variables q,p,ζ of (14) and in the original Nosé variables Q,P,P_s of (11). Projections onto the q-p coordinate—momentum plane and the ζ-p friction variable—momentum plane are also drawn. The full $qp\zeta$ trajectory is a simple twisted loop characterized by a single maximum of p. A moderate variation of the initial conditions results in a torus such as that depicted in Fig. 1.

If the perturbation α is increased to $\alpha = 10$, the simplest possible reentrant mode again shows one maximum in p as is reproduced in Fig. 3. By decreasing p_0, however, it is possible to generate modes with up to $n = 6$ maxima of p. The case $n = 5$ is plotted in Fig. 4.

If α is increased further, the situation does not change qualitatively except that orbits with a much larger n be-
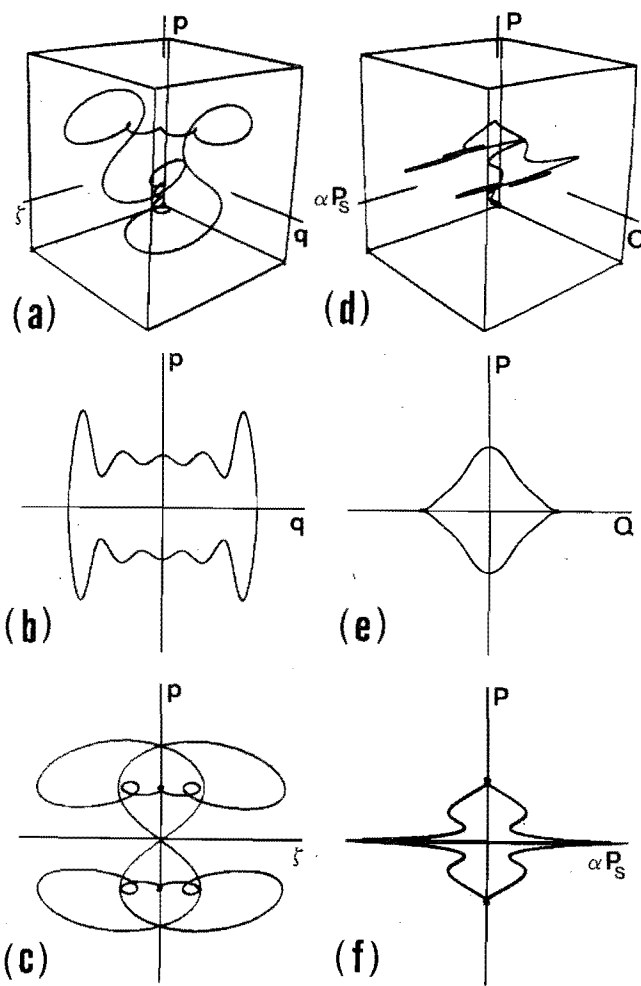
come possible. This is demonstrated in Figs. 5–7 for $\alpha = 100$ and $n = 1, 9$, and 19, respectively. The different appearance of the trajectories in the q,p and Q,P,s,P_s representations is striking. The initial conditions for reentrant orbits and the times τ_0 required by the oscillator to complete a full cycle using (14) are listed in Table I.

Our results show that reentrant trajectories with winding ratio zero may be classified in terms of the number of turning points of p and q or, alternatively, by the number n of maxima of p. These orbits are stable in the sense that the numbers of oscillations or of turning points are not changed by small variations in the starting conditions or in the friction strength α.

In the limit of large perturbation α the periodic orbits have a particularly simple appearance and are partially amenable to an analytic solution. We consider two limiting cases.

Case 1. $\alpha \gg 1$, p close to 1. These conditions are met by the high-frequency limit illustrated in Fig. 7. Putting
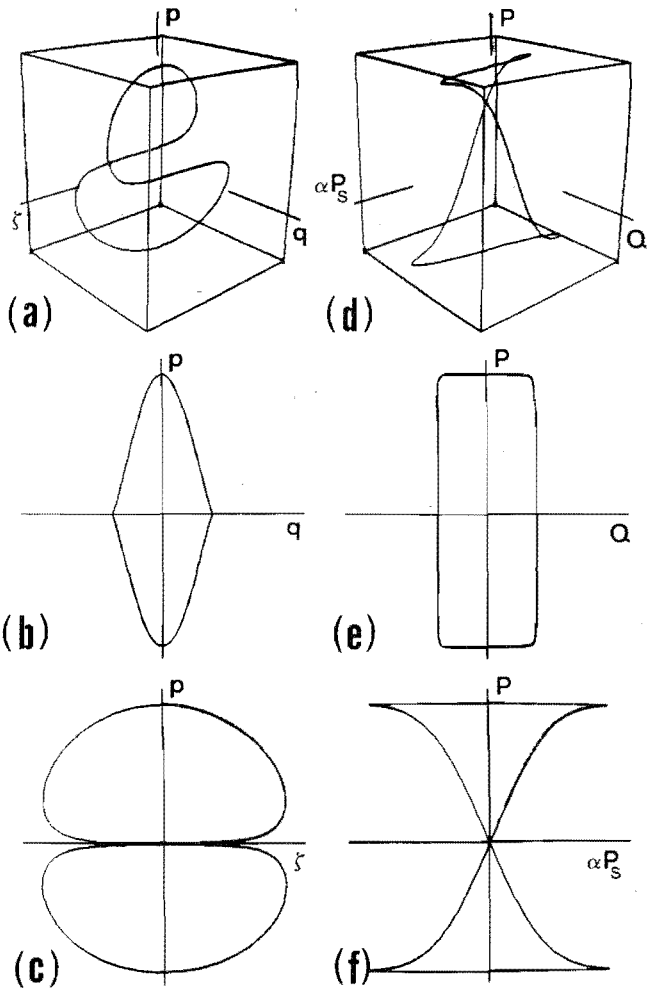
FIG. 5. As in Fig. 2 for $\alpha = 100$ and $n = 1$. Initial condition: (a)−(c), $q_0 = 0$, $p_0 = 3.16$, $\zeta_0 = 0$; (d)−(f), $Q_0 = 0$, $P_0 = 3.16$, $s_0 = 1$, $P_{s0} = 0$. Scales: (a)−(c), $-0.5 \leq q \leq 0.5$, $-3.5 \leq p \leq 3.5$, $-30 \leq \zeta \leq 30$; (d)−(f), $-0.5 \leq Q \leq 0.5$, $-3.5 \leq P \leq 3.5$, $-30 \leq \alpha P_s \leq 30$.
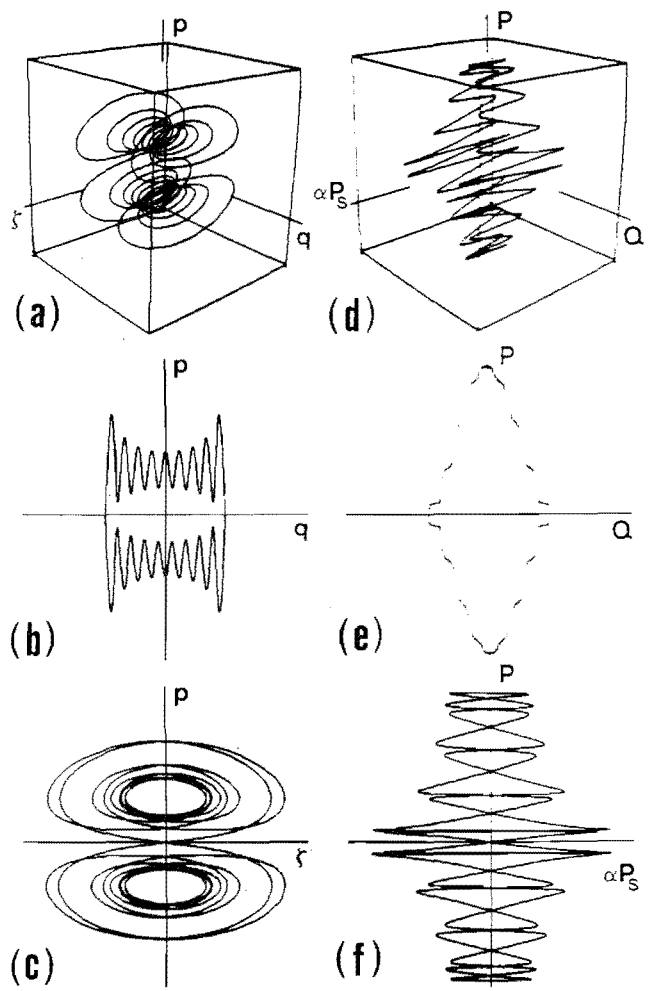

FIG. 6. As in Fig. 2 for $\alpha = 100$ and $n = 9$. Initial condition: (a)−(c), $q_0 = 0$, $p_0 = 1.43$, $\zeta_0 = 0$; (d)−(f), $Q_0 = 0$, $P_0 = 1.43$, $s_0 = 1$, $P_{s0} = 0$. Scales: (a)−(c), $-4.5 \leq q \leq 4.5$, $-3.5 \leq p \leq 3.5$, $-20 \leq \zeta \leq 20$; (d)−(f), $-4.5 \leq Q \leq 4.5$, $-1.5 \leq P \leq 1.5$, $-20 \leq \alpha P_s \leq 20$.

$$p = 1 + \delta, \quad \delta \ll 1 , \tag{16}$$

and using the initial conditions $q_0 = 0$, $p_0 = 1 + \delta_0$, $\zeta_0 = 0$, the equations of motion (14) yield

$$\dot{\zeta} = 2\alpha\delta, \quad q = t + \zeta/2\alpha . \tag{17}$$

Furthermore,

$$\ddot{\delta} + 2\alpha\delta + 1 = 0 . \tag{18}$$

The solution to these equations to order δ and $1/2\alpha$ is given by

$$q = t + \frac{\delta_0}{\sqrt{2\alpha}} \sin(\sqrt{2\alpha}t) ,$$
$$p = 1 + \delta_0 \cos(\sqrt{2\alpha}t) , \tag{19}$$
$$\zeta = -t + \delta_0\sqrt{2\alpha}\sin(\sqrt{2\alpha}t) ,$$

This represents an orbit spiralling around the axis

$p = 1$, $\zeta = -q$, as is easily verified also from Figs. 7(a)−7(c). As we change to the original Nosé variables according to (12), we find (to the same order of $1/2\alpha$ and δ)

$$Q = t + \frac{\delta_0}{\sqrt{2\alpha}} \sin(\sqrt{2\alpha}t) ,$$
$$P = (1 + \delta_0)\exp(-t^2/2) ,$$
$$s = \exp(-t^2/2)\{1 + \delta_0[1 - \cos(\sqrt{2\alpha}t)]\} , \tag{20}$$
$$\alpha P_s = -t + \delta_0\sqrt{2\alpha}\sin(\sqrt{2\alpha}t) .$$

Except for modulations of order δ_0, a plot of P versus Q reveals a Gaussian $\exp(-Q^2/2)$ which is verified also by the numerical solution of (11) as shown in Fig. 7(e).

Case 2. $\alpha \gg 1$ and $p^2 \gg 1$. This case is met by Fig. 5. Neglecting 1 as compared to p^2 in (14), the energy $E' = q^2/2 + p^2/2 + \zeta^2/2\alpha$ is a constant of the motion. The trajectory moves on the surface of an ellipsoid with the main axes of lengths $\sqrt{2E'}, \sqrt{2E'}, \sqrt{2\alpha E'}$ along the
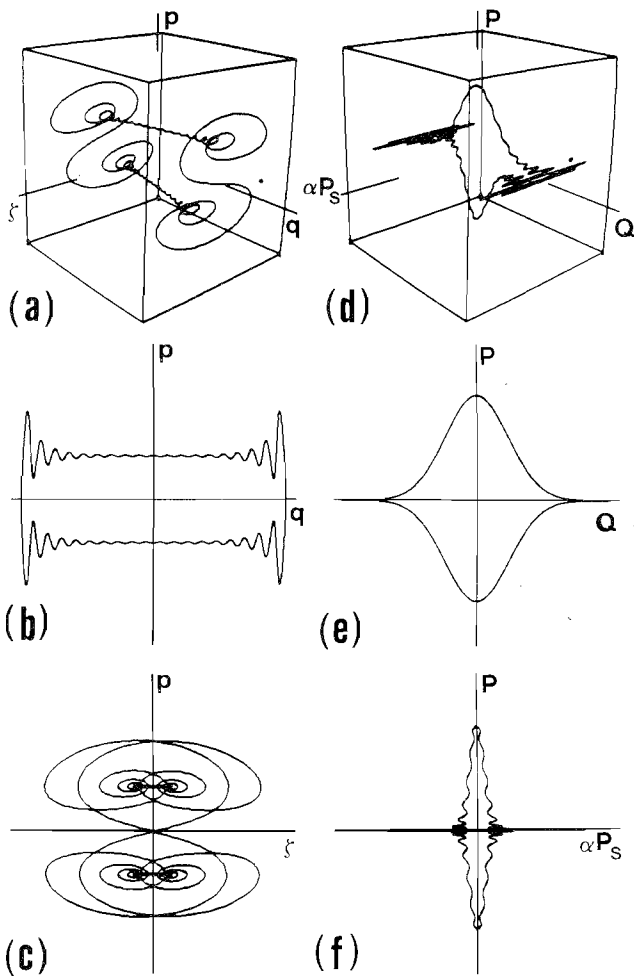
(a) **(d)**

(b) **(e)**

(c) **(f)**

FIG. 7. As in Fig. 2 for $\alpha = 100$ and $n = 19$. Initial condition: (a)–(c), $q_0 = 0$, $p_0 = 1.0085$, $\zeta_0 = 0$; (d)–(f), $Q_0 = 0$, $P_0 = 1.0085$, $s_0 = 1$, $P_{s0} = 0$. Scales: (a)–(c), $-4.5 \leq q \leq 4.5$, $-3.5 \leq p \leq 3.5$, $-20 \leq \zeta \leq 20$; (d)–(f), $-4.5 \leq Q \leq 4.5$, $-1.5 \leq P \leq 1.5$, $-20 \leq \alpha P_s \leq 20$.

q,p,ζ frame of reference, respectively. For this case, (14) can be simplified, and the resulting equations

$$\dot{q} = p, \quad \dot{p} = -\zeta p, \quad \dot{\zeta} = \alpha p^2 \tag{21}$$

have the solution

$$p/p_0 = \mathrm{sech}(\eta t) \ ,$$

$$\zeta/\eta = \tanh(\eta t) \ , \tag{22}$$

$$\tan(\sqrt{\alpha} q) = \sinh(\eta t) \ ,$$

where the relaxation rate η is $\sqrt{\alpha} p_0$, and p_0 is the initial momentum. These equations describe the motion in parts (b) and (c) of Fig. 5, replacing the figure-eight in part (c) by its limiting large α form, an ellipse. These "large α" relations describe only the "large p" portion of parts (c) and (f) of Fig. 5.

TABLE I. Initial condition for reentrant Nosé harmonic-oscillator orbits, $q_0 = 0$, p_0, $\zeta_0 = 0$, for three perturbations α. The integer n measures the number of p maxima, and τ_0 is the time required for the oscillator to complete a full cycle using (14).

α	n	p_0	τ_0
1	1	1.55	5.58
10	1	2.25	3.25
	3	1.44	8.66
	5	1.036	14.10
	6	0.925	17.92
	4	0.72	11.31
	2	0.27	6.06
100	1	3.16	1.36
	3	2.51	3.58
	5	2.04	5.38
	7	1.69	7.02
	9	1.43	8.62
	11	1.25	10.25
	13	1.135	11.92
	15	1.068	13.63
	17	1.028	15.36
	19	1.0085	17.11

IV. HARMONIC-OSCILLATOR NOSÉ MECHANICS: CHAOTIC TRAJECTORIES

For sufficiently large α the regions of phase space in which regular orbits are possible are surrounded by regions in which the oscillator generates chaotic trajectories. In Fig. 8(a) a perspective view of such a trajectory in the first octant is shown. The complexity of this structure changes as α is increased. It can be studied by constructing Poincaré maps of sections for the plane $q = 0$. In such a map, regular trajectories produce either a finite string of dots along the surface of a KAM torus, if the winding ratio is a rational number, or a closed loop for irrational winding ratios. Chaotic trajectories generate instead a filled or at least fractal region with dimensionality greater than two and dimensionality greater than one in the Poincaré map.

In Fig. 9 a series of such Poincaré sections for increasing α in the $qp\zeta$ representation of (14) is shown. It should be stressed that these maps are independent of the value of the Hamiltonian and, consequently, of the initial conditions as long as the latter are in the big stochastic domain of the phase space. In principle, the Poincaré sections of Fig. 9 cover an infinite range rather than finite range of the $p\zeta$ plane. This can be traced to the presence of the logarithmic term in the Nosé Hamiltonian (10). In this respect there is a difference between the Nosé oscillator and the Henon-Heiles and the double-pendulum cases mentioned before. In practice, however, the oscillator's $qp\zeta$ trajectory remains in the vicinity of the origin for times accessible to numerical simulations. This is demonstrated in Fig. 8(b), where a chaotic trajectory with wild initial conditions is followed for a long time and on a large scale. It behaves like a strange attractor familiar
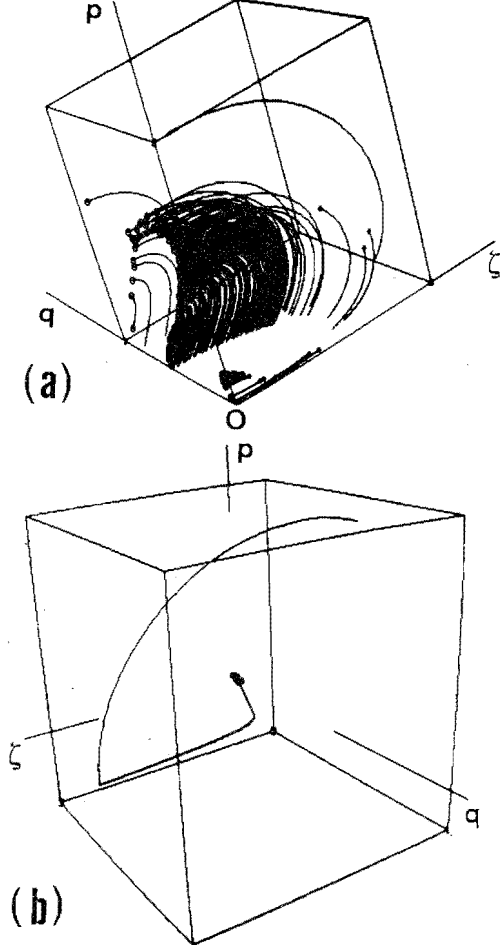
FIG. 8. (a) Perspective view of a chaotic trajectory of the Nosé oscillator in the first octant of phase space for $\alpha = 1.5$. Initial condition: $q_0 = 0$, $p_0 = 5$, $\zeta_0 = 0$. The range of scales marked by the cube is $0 \leq q \leq 3$, $0 \leq p \leq 5$, $0 \leq \zeta \leq 5$. (b) Perspective view of a chaotic trajectory in phase space for $\alpha = 10$. Initial condition: $q_0 = 150$, $p_0 = 200$, $\zeta_0 = -200$. The range of scales marked by the cube is $-200 \leq q \leq 200$, $-200 \leq p \leq 200$, $-500 \leq \zeta \leq 500$. The trajectory is followed for times $t \leq 3000 (= 3 \times 10^7$ time steps). The constant of the motion (6), $H = 33250$, varies along the trajectory by less than 0.02.

FIG. 9. Poincaré map of sections p vs ζ at $q = 0$ for the Nosé oscillator. The pictures are obtained for the same constant of the motion, but for different values of the perturbation α. Initial condition: $q_0 = 0$, $p_0 = 5$, $\zeta_0 = 0$. Parameters and range of scales: (a) $\alpha = 0.66$; $-5 \leq \zeta \leq 5$, $-4 \leq p \leq 4$; (b) $\alpha = 1$; $-5 \leq \zeta \leq 5$, $-5 \leq p \leq 5$; (c) $\alpha = 1.5$; $-5 \leq \zeta \leq 5$, $-5 \leq p \leq 5$; (d) $\alpha = 3$; $-5 \leq \zeta \leq 5$, $-5 \leq p \leq 5$; (e) $\alpha = 10$; $-10 \leq \zeta \leq 10$, $-5 \leq p \leq 5$; (f) $\alpha = 100$; $-30 \leq \zeta \leq 30$, $-4 \leq p \leq 4$.

from the study of dissipative systems. Since the Nosé-oscillator problem basically derives from the Hamiltonian (10) we use the term "strange attractor" merely to characterize our experimental findings. If any of the variables involved can be practically infinite on the energy shell the system cannot possibly be ergodic within finite time.

In Fig. 9 there are large enclosed islands of stability accessed by regular orbits (periodic and quasiperiodic). Each big island is possibly subdivided further by thin chaotic sheets[21] which separate different regular KAM solutions. Since these chaotic sheets—if they exist—are disconnected from the big chaotic sea, they would not show up in the Poincaré maps of Fig. 9. In this paper we restrict ourselves to the study of the chaotic sea. Particularly for small values of α, the big islands of stability are separated by rather thin walls of the chaotic domain. This can also be visualized from the plot of Fig. 8(a).
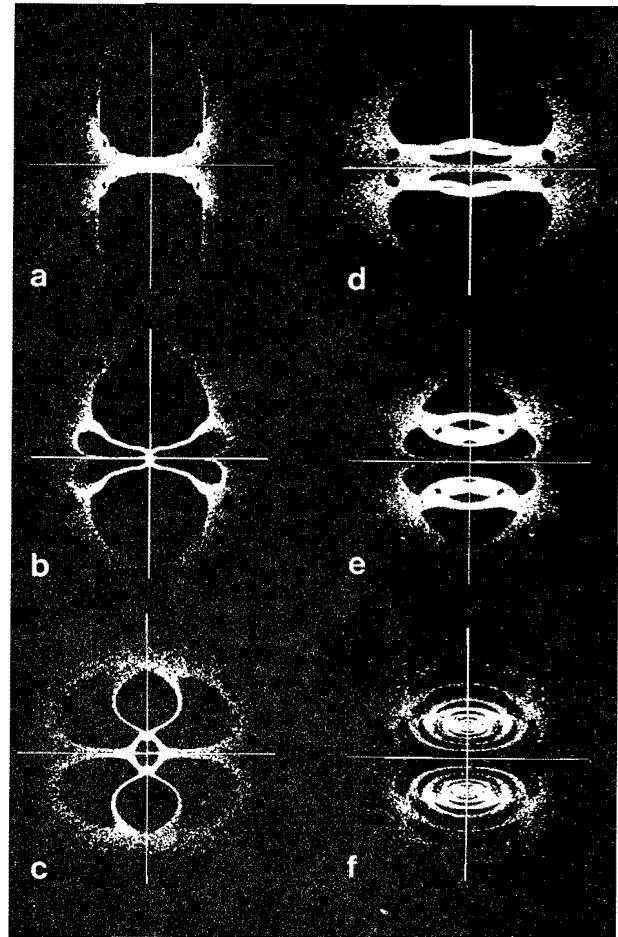
These walls move with changing α, which may lead to rather dramatic changes in the appearance of the Poincaré map. With increasing α the number of stability islands increases. Each such island may be indexed by the number n of maxima of p of the corresponding regular orbits.

Let us turn briefly to the question of how chaotic motion is generated. In Fig. 10(a) a projection of a stochastic trajectory ($\alpha = 10$) onto the pq plane is shown. For short-time intervals the trajectory follows the "dogbone" pattern similar to that of regular trajectories familiar from Figs. 2(b)–7(b). For large enough α, switching between different patterns may occur. In this case the chaotic motion may be viewed as a bifurcation phenomenon mixing almost reentrant modes. The same situation in terms of the original Nosé variables is shown in Fig. 10(b).

We may construct Poincaré maps of sections ($Q = 0$) also in the $QPsP_s$ representation of (11). For Q equal to zero, the condition for the Poincaré section, and P_s fixed, the maximum value of P can be achieved by maximizing
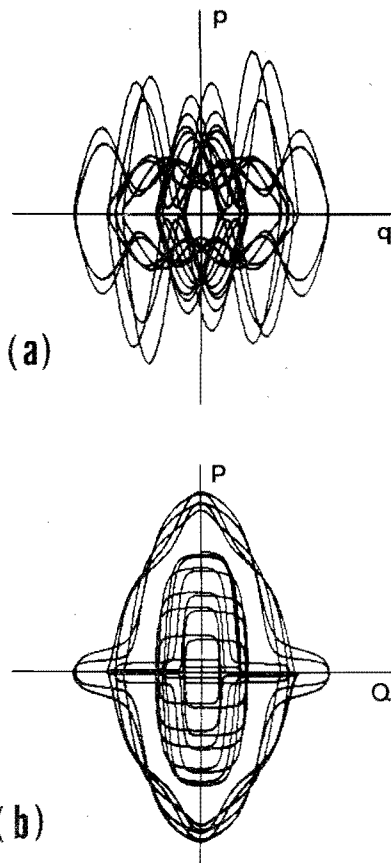
$$-\zeta = \frac{\partial \dot{q}}{\partial q} + \frac{\partial \dot{p}}{\partial p} + \frac{\partial \dot{\zeta}}{\partial \zeta} = \frac{d \ln V}{dt} \ . \tag{24}$$

This measure of the changing phase-space volume seems not to be related to the Lyapunov instability or fractal dimensionality. Fundamentally, our system is described by Hamiltonian mechanics. Thus the expansion and contraction of the phase volume, described in terms of scaled variables, is only a result of the changed time scale and has no fundamental physical significance.

The stochasticity present in a strange attractor can be described[22] in terms of its Hausdorff dimension and the Lyapunov exponents. In the following we outline the estimation of these or related quantities for the Nosé oscillator.

A. The fractal dimension

A quantity closely related to the fractal dimension is the correlation exponent introduced by Grassberger and Procaccia.[22,23] It is defined by the power-law dependence of the correlation integral
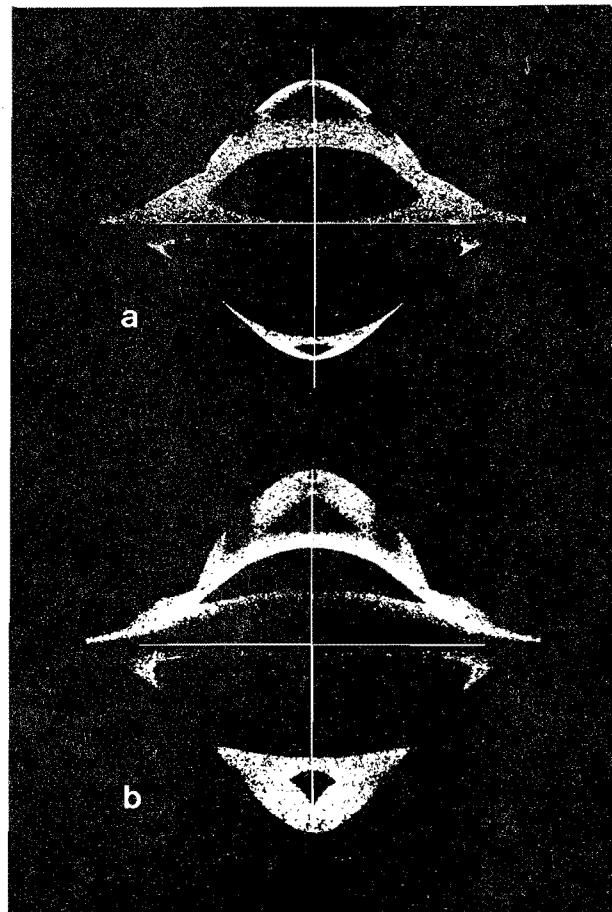

(a)

(b)

FIG. 10. Projection of a short part of a chaotic trajectory of the Nosé oscillator onto the (a) q,p plane (scale: $-3.5 \leq q \leq 3.5$, $-5 \leq p \leq 5$) and (b) Q,P plane (scale: $-3.5 \leq Q \leq 3.5$, $-3 \leq P \leq 3$) for $\alpha = 10$ and the initial condition $q_0 = 0$, $p_0 = 1.75$, $\zeta_0 = 0$.

the Hamiltonian (10). From $\partial H_N / \partial s = 0$ at constant Q and P_s we obtain

$$P = s = \exp(H_N - \alpha P_s^2 / 2 - \tfrac{1}{2}) \ . \tag{23}$$

Thus a Poincaré map for $Q = 0$ in the original Nosé representation is bounded in the P direction by a Gaussian in contrast to the unbounded $qp\zeta$ case of Fig. 9. In Fig. 11(a) a Poincaré section ($Q = 0$) for $\alpha = 10$ is reproduced, where we have plotted $\text{sgn}(|P| - s)|P|$ instead of P. This helps to distinguish between the cases $|P| \geq s$ (dots in the upper half of the Poincaré plane) and $|P| < s$ (lower half). In order to establish a correspondence between these different representations, it is convenient to modify Fig. 9 by plotting $\text{sgn}(|p| - 1) \times \min(|p|, 1/|p|) \exp(-\zeta^2 / 2\alpha)$—instead of p—versus ζ for $q = 0$. A comparison of such a plot in Fig. 11(b) with Fig. 11(a) shows a close correspondence between these two different representations.

It is useful to notice that, for fixed ζ, the equations of motion (14) are those of a damped oscillator ($\zeta > 0$) or an exponentially unstable oscillator ($\zeta < 0$). Motion in the ζ direction produces trajectories with $\langle \zeta \rangle$ equal to zero composed of expanding parts and contracting parts. ζ is a direct measure of the (comoving, or "Lagrangian") rate of contraction of the phase-space volume, the Lie derivative:

FIG. 11. Poincaré map of sections for the Nosé oscillator for $\alpha = 10$. (a) In the original Nosé variables: Any cut of the trajectory through the $Q = 0$ plane generates a point $(\alpha P_s, |P|)$, if $|P| \geq s$, and a point $(\alpha P_s, -|P|)$, if $|P| \leq s$. Scales: $-6 \leq \alpha P_s \leq 6$, $-2 \times 10^5 \leq$ ordinate $\leq 2 \times 10^5$. (b) In the modified $qp\zeta$ variables: Any cut through the $q = 0$ plane generates a point $(\zeta, |p|^{-1} \exp(-\zeta^2 / 2\alpha))$, if $|p| \geq 1$ (upper half of the plane) and a point $(\zeta, -|p| \exp(-\zeta^2 / 2\alpha))$, if $|p| < 1$ (lower half). Scales: $-6 \leq \zeta \leq 6$, $-1 \leq$ ordinate ≤ 1.

$$C(R) = \int_0^R d\mathbf{X} g(\mathbf{X}) \sim R^\nu , \qquad (25)$$

where the pair-distribution function $g(\mathbf{X})$ is the probability density of finding two randomly chosen points on an attractor with a phase-space separation $\mathbf{X}$. It may be approximately calculated from

$$g(\mathbf{X}) = \frac{1}{N(N-1)} \sum_{\substack{i \\ i \neq j}} \sum_j \delta(\mathbf{X} + \mathbf{X}_i - \mathbf{X}_j) , \qquad (26)$$

where the $\mathbf{X}_i$ denote a series of N phase-space points on the trajectory separated in time by equal time intervals τ. Using the algorithm of Ref. 22 we have evaluated $C(R)$ for the Nosé oscillator in the $qp\zeta$ representation for selected values of α. The results are given in Fig. 12. The scaling relation (25) is well obeyed over a large range of distances R for intermediate α values around 3. This condition corresponds also to large values of the Lyapunov exponent λ. If the phase space accessible to the chaotic trajectory has a sheetlike structure such as for $\alpha = 1$ [Fig. 9(b)], this distance range R, for which the scaling relation (25) holds, is drastically reduced. The straight lines in

Fig. 12 for α larger than 0.1 fit the experimental data well in the distance range in which scaling is expected to hold. Their slopes are consistent with a fractal dimension d equal to 3 in view of the fact that ν is a lower bound of d. This indicates that the trajectories of the Nosé oscillator are phase-space filling and—at least from the standpoint of fractal dimensionality—could be canonical.

The curve for $\alpha = 0.1$ in Fig. 12 corresponds to a regular trajectory. It scales according to a dimensionality $\nu = 2$ for small values of R (dashed line in Fig. 12) and $\nu = 1$ for large R reflecting the properties of a torus.

B. The Lyapunov instability

The exponential divergence of two nearby trajectories in three-dimensional phase space can be described by the three Lyapunov exponents. We have evaluated the largest exponent, henceforth denoted by λ, for a whole range of α values (see Fig. 13). In the original method by Benettin et al. of calculating,[24,21] two trajectories separated by d_0 at $t = 0$ are followed in phase space. The second trajectory is kept close to the "reference trajectory" by periodically rescaling its phase-space coordinates to reduce the offset length to d_0 (method A). Another procedure by Contopoulos et al.[25] avoids rescaling by solving simultaneously the equations of motion and the corresponding variational system for a single trajectory (method B). However, for large time t the variables of the variational system assume extremely large values which again necessitates periodic rescaling. We have used still another method described in more detail in Ref. 26, which solves the equations of motion for two neighboring trajectories, where the phase-space offset of trajectory 2 is kept constant in absolute value by adding a constraint force to its equation of motion (method C). If $X_2 = (q_2, p_2, \zeta_2)$ denotes a phase point on trajectory 2, this gives

$$\dot{\mathbf{X}}_2 = \dot{\mathbf{X}}_2(\mathbf{X}_2) - \beta(\mathbf{X}_2 - \mathbf{X}_1) , \qquad (27)$$

where

$$\beta = \frac{(\mathbf{X}_2 - \mathbf{X}_1) \cdot [\dot{\mathbf{X}}_2(\mathbf{X}_2) - \dot{\mathbf{X}}_1]}{(\mathbf{X}_2 - \mathbf{X}_1) \cdot (\mathbf{X}_2 - \mathbf{X}_1)} . \qquad (28)$$
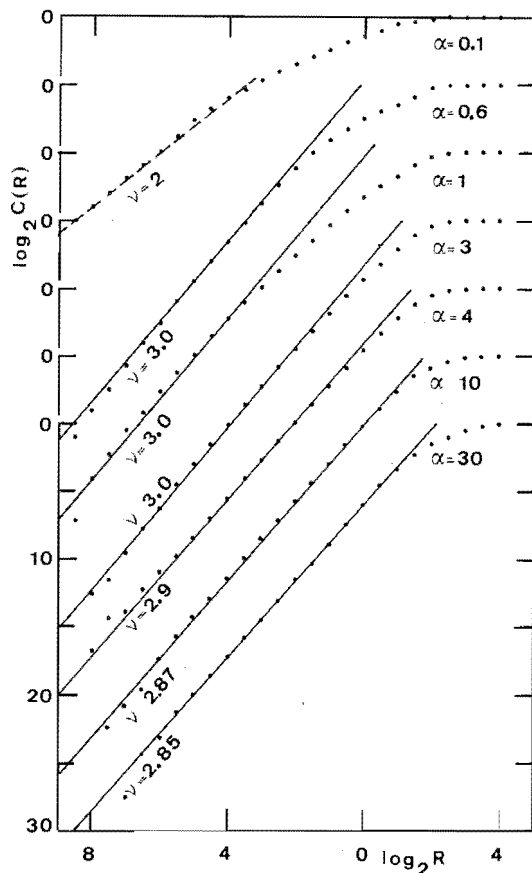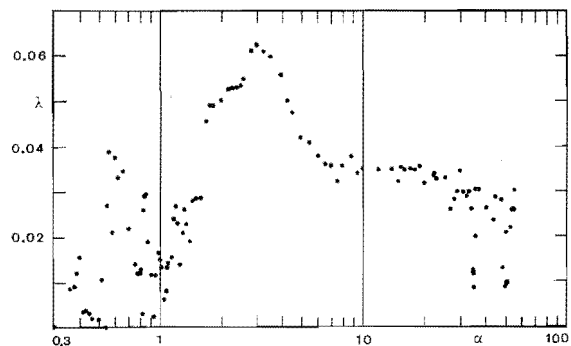

FIG. 12. Dependence of the correlation integral $C(R)$ on the upper integration limit R of Eq. (23) for various perturbations α of chaotic Nosé-oscillator trajectories with initial condition $q_0 = 0$, $p_0 = 5$, $\zeta_0 = 0$. Parameters of the simulations: $\alpha = 0.6$; $N = 20\,000$, $\tau = 1000\Delta t = 5$; $\alpha = 1.0$; $N = 25\,000$, $\tau = 1000\Delta t = 5$; $\alpha = 3.0$; $N = 20\,000$, $\tau = 1000\Delta t = 5$; $\alpha = 4.0$; $N = 15\,000$, $\tau = 1000\Delta t = 5$; $\alpha = 10.0$; $N = 20\,000$, $\tau = 2000\Delta t = 6$; $\alpha = 30.0$; $N = 20\,000$, $\tau = 1000\Delta t = 2$.

FIG. 13. Lyapunov exponents λ as a function of the perturbation parameter α for given constant of the motion ($H = 12.5$; $q_0 = 0$, $p_0 = 5$, $\zeta_0 = 0$) of the Nosé oscillator. The time step Δt used for the simulation varied from 0.05 for $\alpha < 10$ to 0.001 for $\alpha = 100$. At least 10^7 time steps are calculated for each point.

The unconstrained equations of motion follow from (14):

$$\dot{\mathbf{X}}_2(\mathbf{X}_2) = \begin{cases} p_2 \\ -q_2 - \zeta_2 p_2 \\ \alpha(p_2^2 - 1) . \end{cases} \tag{29}$$

If the trajectories are followed for a time T, the Lyapunov exponent may be calculated from the average

$$\lambda = \left\langle \ln \left| \frac{1}{1-\beta} \right| \right\rangle \approx \langle \beta \rangle = \frac{1}{T} \int_0^T \beta \, dt . \tag{30}$$

This average is most conveniently evaluated by augmenting the equations of motion for the two trajectories with an additional equation integrating β with respect to time. Using a fourth-order Runge-Kutta algorithm,[20] the convergence of this method is demonstrated in Fig. 14. The integration steps may be chosen much larger for this method than for the original algorithm employing periodic rescaling. In all simulations an offset distance $d_0 \leq 0.001$ is used. The estimated accuracy is 2% for large values of λ and 6% otherwise. If the Lyapunov exponents are plotted as a function of the coupling strength α (Fig. 13), a rather complicated picture emerges. The magnitude of λ is related to the width of the chaotic regime in the Poincaré maps of Fig. 9, a voluminous stochastic sea corresponding to a large Lyapunov instability. The deep minima in Fig. 13 are possibly due to tiny islands of stability which make themselves felt by a lowering of λ for trajectories passing near the boundary between chaotic and regular regimes. Probably many more minima exist than are discovered and depicted in Fig. 13. How the breakdown of the scaling relation (25) for large values of R is affected by the appearance of these islands of stability remains to be examined.
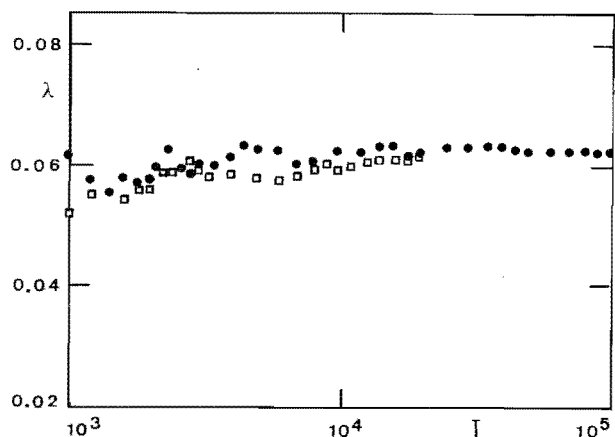

FIG. 14. Convergence of time averages of the Lyapunov exponents of the Nosé oscillator for $\alpha = 3$ ($q_0 = 0$, $p_0 = 5$, $\zeta_0 = 0$). Open squares: method employing periodic rescaling of the trajectory offset d of trajectory 2 to $d_0 = 0.003$ every 50th time step $\Delta t = 0.001$. Closed circles: constraint force method Eqs. (25)–(28) for $d_0 = 0.003$ and a time step $\Delta t = 0.01$.

V. TWO-DIMENSIONAL CHAOTIC PROBLEMS WITH FIVE- AND THREE-DIMENSIONAL PHASE SPACES

The lack of chaotic behavior in some regions of the single-oscillator phase space shows that Nosé's equations of motion need not produce a canonical phase-space distribution. Various few-particle modifications of the single-oscillator calculation using nonlinear forces failed to pass simple moment tests for Gaussian distributions in the friction variable or the kinetic energy K. Thus several distinct kinds of one-dimensional systems are not sufficiently chaotic to distribute a typical initial state over the entire phase space.

On the other hand, the oscillation of the ideal-gas kinetic energy according to Eqs. (8) and (9) suggests that an interaction with a mechanism for shifting the phase and amplitude of the kinetic-energy oscillation could link together all energy shells, resulting in a canonical distribution. We therefore studied in some detail a system with two particles in a plane with periodic boundary conditions. The dynamics of such a system in relative coordinates $\mathbf{r} = \mathbf{q}_2 - \mathbf{q}_1$ is the same as the dynamics of the cell model,[27] in which a particle with a reduced mass $\mu = m_1 m_2/(m_1 + m_2)$ interacts with a fixed lattice of neighbors. The particle diameter is denoted by σ.

It is convenient to introduce reduced units with μ, σ, and $D k_B T$ acting as units of mass, length, and energy, respectively. The specific model studied is a square cell of area 4 with one particle fixed at the cell corners and the other being free to move throughout the cell. The potential energy is taken as

$$\Phi = \begin{cases} 3(1-r)^4, & r \leq 1 \\ 0, & r > 1. \end{cases} \tag{31}$$

The equations of motion, with $\alpha = 1$, follow from (5):

$$\dot{\mathbf{r}} = \mathbf{p}, \quad \dot{\mathbf{p}} = \mathbf{F} - \zeta \mathbf{p}, \quad \dot{\zeta} = \mathbf{p}^2 - 2 , \tag{32}$$

with the provision that the force $\mathbf{F}$ is periodic in both the x and y directions with periodicity equal to two, the cell length. The numerical integration was carried out with an accuracy such that the constant of the motion [as derived from (6)]

$$H = \Phi + \mathbf{p}^2/2 + \zeta^2/2 + 2 \int_0^t \zeta(t') dt' \tag{33}$$

drifted by about one part in 10^7 per complete collision (free streaming followed by interparticle interaction). Figure 15 shows the geometry of the problem and a short stretch of a trajectory. If this system had a canonical distribution proportional to $\exp(-\Phi - \mathbf{p}^2/2 - \zeta^2/z)$ then the moments of the kinetic energy $K = (p_x^2 + p_y^2)/2$ and of the friction ζ would be $\langle K \rangle = 1$, $\langle K^2 \rangle = 2$, $\langle \zeta^2 \rangle = 1$, and $\langle \zeta^4 \rangle = 3$. The numerical results for these quantities after 10^4 collisions were 1.00, 2.01, 1.01, and 3.18, respectively. The relatively large fluctuations found in these two-particle calculations suggest that these values are consistent with the canonical distribution. In Fig. 16 the normalized distribution of ζ is shown. It is in good agreement with the Gaussian distribution.
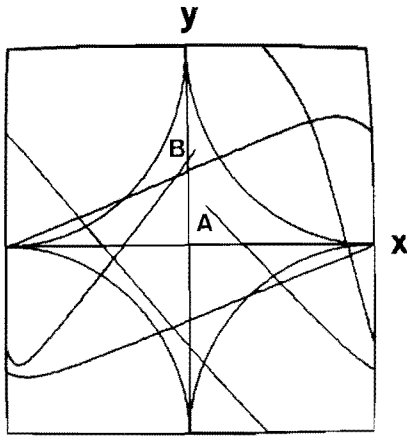
We conclude that in a system with a mechanism for

FIG. 15. Geometry—in relative coordinates $\mathbf{r}=\mathbf{q}_2-\mathbf{q}_1=(x,y)$—of the "two-particle" Nosé dynamics in a square cell of side length 2 with periodic boundary conditions. The quarter circles of radius 1 centered at the corners indicate the boundaries for interparticle interaction, particle 1 being fixed to the corners. A short portion of a trajectory beginning at point A and ending at point B is also shown ($\alpha=1$, $x_0=0.1$, $y_0=0.2$, $p_{x0}=1$, $p_{y0}=-1$, $\zeta_0=0$).

FIG. 16. Distribution of ζ in the two-particle Nosé system. Solid line, simulation result; dashed line, theoretical (Gaussian) distribution.

enhancing instability by velocity scattering off a convex surface and with a phase-shifting free-flight region (the region outside the quarter-circle sections of Fig. 15 in the one-particle case moving in a periodic lattice) the canonical distribution will be achieved. Thus almost any interesting system should follow the canonical distribution.

It is difficult to make extremely long runs of high accuracy in two or three dimensions, but we take the near constancy of the constant of the motion H as an indication that our results are typical of the actual behavior of Nosé dynamics. Our failure to detect any noncanonical behavior of the Nosé two-dimensional problem led to the study of an even simpler system with a three-dimensional phase space, the Gaussian-dynamics limit of the Nosé problem. Gauss's principle of least constraint leads to the same equations of motion for $\mathbf{r}$ and $\mathbf{p}$ as Nosé's,

$$\dot{\mathbf{r}}=\mathbf{p}, \quad \dot{\mathbf{p}}=\mathbf{F}-\zeta\mathbf{p} . \tag{34a}$$

But ζ, according to Gauss, is an explicit function of the coordinates and momenta,[2,28]

$$\zeta=(\mathbf{p}\cdot\mathbf{F})/(\mathbf{p}\cdot\mathbf{p}) . \tag{34b}$$

With this choice the kinetic energy is a constant of the motion, and the velocity space in two dimensions is contracted to the perimeter of a circle. We may ask whether or not the distribution in configuration subspace is canonical, i.e., whether it has the form $\sim\exp(-\Phi/p^2)$. With the potential of Eq. (31) the various moments of the potential energy Φ and of the friction ζ should then be $\langle\Phi\rangle=0.14$, $\langle\Phi^2\rangle=0.11$, $\langle\Phi^4\rangle=0.22$, $\langle\zeta^2\rangle=0.78$, and $\langle\zeta^4\rangle=10.0$. A long simulation of the isokinetic motion involving 9000 collisions yielded the respective values 0.16, 0.12, 0.24, 0.88, and 10.9. Keeping the statistical uncertainties in mind, we have to conclude that the
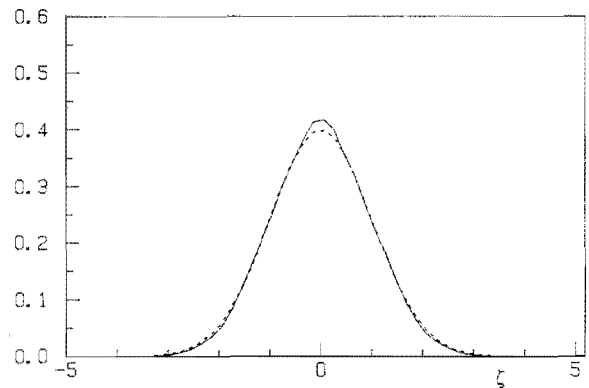
Gaussian system is probably consistent with a canonical distribution in configuration space.

VI. SUMMARY AND CONCLUSIONS

The Nosé oscillator falls in a broad category of problems which are not sufficiently chaotic to fill their available phase spaces. It has relatively many interesting limiting cases and relatively complicated Poincaré sections, but otherwise mostly reinforces the idea that small systems do not follow a statistical-mechanical average over accessible states.

On the other hand, the two-dimensional calculations indicate that only slightly more complicated systems probably do fill their phase spaces in a quasiergodic way. A careful study of the two-soft-disk system, using Nosé dynamics in a phase space with five variables, led to no evidence for the failure of statistical mechanics. This suggested an even simpler system, in principle not more complicated than the Nosé oscillator. This two-soft-disk system, using Gaussian dynamics in a three-dimensional phase space, still revealed no evidence whatsoever for the strange-attractor behavior associated with the oscillator.

Based on this evidence we would expect that even very simple nonequilibrium systems, or quantum systems, with even more capability for mixing phase space, do indeed fill their phase spaces in an ergodic way.

ACKNOWLEDGMENTS

*Permanent address: Department of Applied Science, University of California at Davis-Livermore, and Lawrence Livermore National Laboratory, Livermore, California 94550.

[1]D. J. Evans and W. G. Hoover, Annu. Rev. Fluid Mech. **18**, 243 (1986).

[2]A. Sommerfeld, *Vorlesungen ueber theoretische Physik; Bd. 1: Mechanik* (Akademische Verlagsgesellschaft Geest und Portig, Leipzig, 1955); L. A. Pars, *A Treatise on Analytical Dynamics* (Oxbow, Woodbridge, Conn., 1979).

[3]D. J. Evans, W. G. Hoover, B. Failor, and B. Moran, Phys. Rev. A **28**, 1016 (1983).

[4]S. Nosé, Mol. Phys. **52**, 255 (1984).

[5]S. Nosé, J. Chem. Phys. **81**, 511 (1984).

[6]M. Ross, J. Chem. Phys. **71**, 1567 (1979); J. P. Hansen and I. R. McDonald, *Theory of Simple Liquids* (Academic, London, 1976).

[7]W. G. Hoover, J. Stat. Phys. **42**, 587 (1986).

[8]A. J. C. Ladd and W. G. Hoover, J. Stat. Phys. **38**, 973 (1985).

[9]G. P. Morriss, Phys. Lett. **113A**, 269 (1985).

[10]W. G. Hoover, B. Moran, and J. Haile, J. Stat. Phys. **37**, 109 (1983).

[11]W. G. Hoover and K. W. Kratky, J. Stat. Phys. **42**, 1103 (1986).

[12]D. N. Zubarev, *Nonequilibrium Statistical Thermodynamics* (Consultants Bureau, New York, 1974), Sec. 27.

[13]G. P. Morriss and D. J. Evans, Mol. Phys. **54**, 629 (1985).

[14]W. G. Hoover, Phys. Rev. A **31**, 1695 (1985).

[15]E. N. Lorenz, J. Atmos. Sci. **20**, 130 (1963); C. Sparrow, *Lorenz Equations: Bifurcations, Chaos and Strange Attractors* (Springer-Verlag, Berlin, 1982).

[16]M. Henon and C. Heiles, Astron. J. **69**, 73 (1964).

[17]P. H. Richter and H.-J. Scholz, in *Stochastic Phenomena and Chaotic Behavior in Complex Systems,* Vol. 21 of *Springer Series in Synergetics,* edited by P. Schuster (Springer-Verlag, New York, 1984); P. H. Richter and H. O. Peitgen, Ber. Bunsenges. Phys. Chem. **89**, 571 (1985).

[18]K. J. Whiteman, Rep. Prog. Phys. **40**, 1033 (1977).

[19]T. P. Coffey and G. W. Ford, J. Math. Phys. **10**, 998 (1969).

[20]B. Carnahan, H. A. Luther, and J. O. Wilkes, *Applied Numerical Methods* (Wiley, New York, 1969).

[21]A. J. Lichtenberg and M. A. Lieberman, *Regular and Stochastic Motion* (Springer-Verlag, New York, 1983).

[22]P. Grassberger and I. Procaccia, Physica **9D**, 189 (1983).

[23]P. Grassberger and I. Procaccia, Phys. Rev. Lett. **50**, 346 (1983).

[24]G. Benettin, L. Galgani, and J.-M. Strelcyn, Phys. Rev. A **14**, 2338 (1976).

[25]G. Contopoulos, L. Galgani, and A. Giorgilli, Phys. Rev. A **18**, 1183 (1978).

[26]W. G. Hoover and H. A. Posch, Phys. Lett. **113A**, 82 (1985).

[27]B. J. Alder, W. G. Hoover, and T. E. Wainwright, Phys. Rev. Lett. **11**, 241 (1963).

[28]W. G. Hoover, Annu. Rev. Phys. Chem. **34**, 103 (1983).